

Waves and air-sea fluxes from a drifting ASIS buoy during the Southern Ocean Gas Exchange experiment

Erik Sahlée,¹ William M. Drennan,² Henry Potter,² and Michael A. Rebozo²

Received 9 March 2012; revised 5 June 2012; accepted 11 June 2012; published 2 August 2012.

[1] The Southern Ocean, while widely acknowledged as playing a major role within the Earth's climate system, remains the most poorly sampled and understood of the world's ocean basins. The High Latitude Surface Flux Working Group of U.S. CLIVAR (Climate Variability and Predictability, part of the World Climate Research Programme) has accordingly identified as a key priority the need for further measurements in the Southern Ocean. During the 2008 Southern Ocean Gas Exchange experiment, an Air-Sea Interaction Spar (ASIS) buoy was deployed to measure air-sea fluxes, surface waves, and mean properties of the upper ocean and lower atmosphere. During its eight-day deployment in the Atlantic sector of the Southern Ocean, the drifting buoy captured two storm events, with winds reaching 20 m s^{-1} and waves approaching 6 m significant height. The wavefield was observed to be dominated by swell waves except for the storm periods. In a combined analysis using data from two other ASIS deployments, existing relations for fetch limited wave growth were evaluated. Measured moisture flux showed good comparison with previous findings indicating a near-constant Dalton number. The drag coefficient was found to be significantly higher than previous parameterization predictions, due to an effect of swell wave interaction with the atmospheric turbulence. This enhanced momentum flux in the swell dominated seas of the Southern Ocean must be accounted for in regional bulk flux relations.

Citation: Sahlée, E., W. M. Drennan, H. Potter, and M. A. Rebozo (2012), Waves and air-sea fluxes from a drifting ASIS buoy during the Southern Ocean Gas Exchange experiment, *J. Geophys. Res.*, *117*, C08003, doi:10.1029/2012JC008032.

1. Introduction

[2] The Southern Ocean (SO) is well known as a major source of uncertainty in both global heat and carbon budget calculations. To a large degree this is due to our lack of knowledge of air-sea transfer processes in the region. This lack of knowledge stems from a dearth of observations both of direct fluxes and of indirect bulk input parameters such as wind speed, as well as a unique environment that does not allow extrapolation of flux estimates from elsewhere. The unique conditions of the SO include consistently high and largely unidirectional winds, high concentrations of sea spray and bubbles, large long-fetch waves and, especially near the continental margin, sea ice.

[3] *Josey et al.* [1999] single out the SO as a region of "very sparse data coverage" in terms of heat fluxes. *Iudicone et al.* [2008, p. 1378] state that "surface buoyancy fluxes in the SO ... are poorly known." This is significant because the SO plays a major role in global thermohaline circulation

(THC) with surface buoyancy acting as a primary driver of THC [*Speer et al.*, 2000; *Iudicone et al.*, 2008]. *Liu et al.* [2011] show the zonal-mean latent heat flux estimates from five well known flux products to vary by a factor of almost two over the entire SO south of 50° S for the period 1989–2005. For sensible heat flux, the models are not even consistent in the sign of the flux. Similarly, in terms of the carbon cycle, *Gruber et al.* [2009, paragraph 5] identify the Southern Ocean as "a region of particularly large discrepancies between different flux estimates," and further comment that this "represents a critical gap in our understanding of the ocean carbon cycle."

[4] Many of the flux studies reported above are referring to flux fields produced using bulk relations along with measured mean meteorological parameters such as wind speed, air and water temperature, and humidity, as well as carbon dioxide concentrations in the water and air. The problems with bulk flux fields in the SO are twofold: first, the bulk relations used to produce the fields [e.g., *Fairall et al.*, 2003] are dominated by measurements taken in much more benign conditions at lower latitudes. Hence the effects of sea spray, thought to be important for heat fluxes [*Andreas*, 1992; *Drennan et al.*, 2007], and bubbles, significant for gas fluxes [*Woolf and Thorpe*, 1991], are not fully accounted for in present bulk relations. Yet these effects may be significant in the high wind regime of the SO. Second, in situ measurements of mean meteorological parameters from ships or

¹Department of Earth Sciences, Uppsala University, Uppsala, Sweden.

²Rosenstiel School of Marine and Atmospheric Science, University of Miami, Miami, Florida, USA.

Corresponding author: W. M. Drennan, Rosenstiel School of Marine and Atmospheric Science, University of Miami, 4600 Rickenbacker Cswy., Miami, FL 33149, USA. (wdrennan@rsmas.miami.edu)



Figure 1. Photograph of the ASIS buoy taken on 10 March 2008 (YD 70), shortly after deployment from the R/V *Ronald Brown*. For reference the mast is 2.4 m high. Photo taken by David Ho.

buoys in the SO are very limited [cf. *Josey et al.*, 1999]. As a result, flux products rely on either satellite or model-derived fields, or on some combination thereof [*Liu et al.*, 2011]. In most cases, however, these satellite fields have not been validated at high latitudes, or at high winds, hence their validity in the SO is uncertain (M. A. Bourassa et al., High-latitude ocean and sea-ice surface fluxes: Challenges for climate research, submitted to *Bulletin of the American Meteorological Society*, 2012).

[5] Direct flux measurements in the SO are very limited. *Banner et al.* [1999] presented momentum, sensible heat and latent heat fluxes measured from an aircraft during the Southern Ocean Waves Experiment, SOWEX. As discussed below, their small data set, collected at 10 m wind speeds up to 20 m s^{-1} , was consistent with previous parameterizations derived in lower wind conditions. More recently, three campaigns focused on gas exchange in the SO: the 2002 Southern Ocean Iron Fertilization experiment (SOFex) [*Wanninkhof et al.*, 2004]; the 2004 SOLAS air-sea gas exchange experiment (SAGE) [*Ho et al.*, 2006; *Harvey et al.*, 2011]; and the 2008 Southern Ocean Gas Exchange experiment (SOGasex) [*Ho et al.*, 2011]. The first two, which included gas flux measurements using the dual tracer method (see below), were carried out in the context of iron fertilization experiments.

[6] SOGasex was the third in a series of U.S. funded field studies aimed at improving our understanding of the processes underlying air-sea gas exchange. The original GasEx campaign took place during June 1998 in the North Atlantic, a large carbon dioxide sink region [*McGillis et al.*, 2001]. The second GasEx experiment took place in winter 2001 in the equatorial Pacific Ocean, one of the largest carbon source regions. The key results included a better understanding of how local non-wind related processes affect gas exchange [*McGillis et al.*, 2004], and CO_2 dynamics [*DeGrandpre et al.*, 2004], *inter alia*.

[7] Here we present the results from the deployment of an Air Sea Interaction Spar (ASIS) buoy [*Graber et al.*, 2000] during SOGasex. The ASIS buoy (see Figure 1) was instrumented to directly measure the air-sea fluxes of momentum, latent heat, carbon dioxide, and aerosol, as well as surface waves, water column properties, and mean meteorology parameters: air temperature, humidity, and wind speed and direction. In section 2 we describe the instrumentation deployed on the ASIS buoy. In section 3 we present the main results, followed by discussion and conclusions in section 4.

2. ASIS During SOGasex

[8] The SOGasex ASIS buoy was deployed from the R/V *Ronald Brown* on 10 March 2008 (year day YD 70) at 50.74° S , 38.5° W . ASIS was deployed within a patch of SF_6/He tracer laid by the ship with the intention of comparing gas exchange rates made by the dual tracer technique [*Nightingale et al.*, 2000] and by eddy covariance using flux sensors on ASIS and the ship. The ASIS buoy was freely drifting with a 10 m drogue attached to its base to reduce the wind influence on the trajectory. Despite the drogue, ASIS soon drifted out of the $O(100 \text{ km}^2)$ tracer patch. Several days after the patch was laid mechanical problems with the *Ronald Brown* necessitated a sudden change in plans with the ship forced to abandon the site during a storm. The ASIS buoy remained in the water throughout the storm, and a second stronger one that followed two days later. When the ship returned to the site after a week only traces of the original patch were located [*Ho et al.*, 2011]. The ASIS buoy, which had drifted 2° eastward, was recovered on 18 March (YD 78) at 50.5° S , 36.1° W . Although a second tracer patch was subsequently released close to the original site, ASIS was not redeployed. The 8-day drift track of ASIS is shown in Figure 2 along with the position of the *Ronald Brown* during the 40-day SOGasex campaign.

[9] To simplify the deployment and recovery of the ASIS buoy from the *Ronald Brown* in the anticipated rough seas, the traditional ASIS mast was shortened by 1.5 m and strengthened, which allowed for the removal of the guy wires. The deck was also opened up to reduce wind resistance, and strengthened. For the drifting experiment three fully redundant ARGOS position beacons (two Seimac Smartcat PTTs and a Telonics TGE-300) were installed. These provide the positions of ASIS at least every hour. The data were used both to locate the buoy and to calculate its drift velocity.

[10] The flux package deployed during SOGasex consisted of a Gill R2A sonic anemometer and a Li-Cor LI-7500 infrared gas analyzer, both installed at the top of the mast with 30 cm vertical separation (see Figure 1). A CLASP

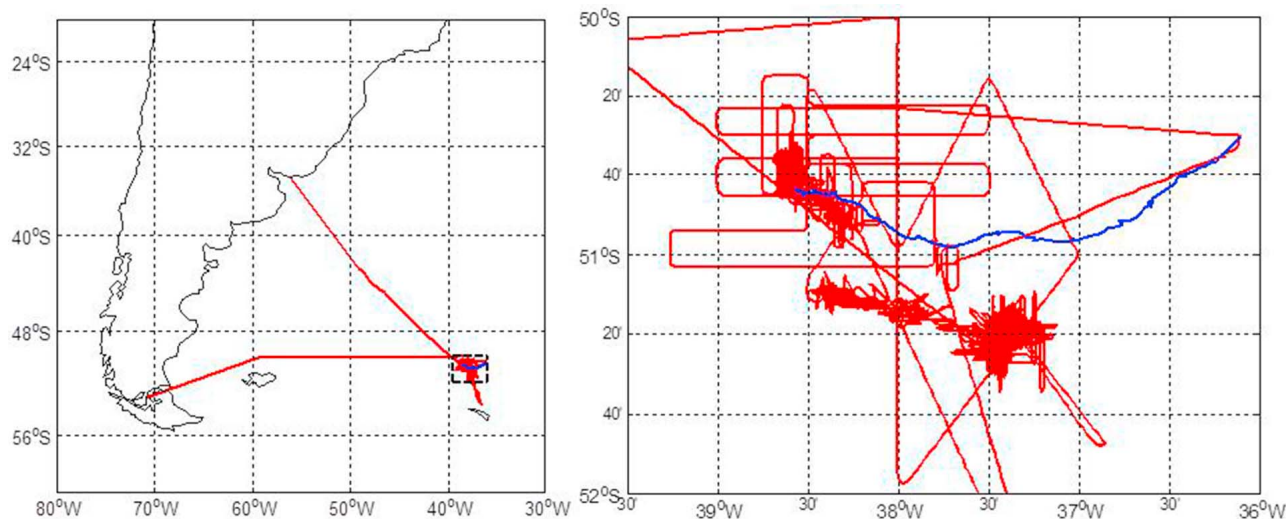


Figure 2. Map of the SOGaseX experimental area: (left) overview and (right) a close-up of the area marked with black dashed lines north of the South Georgia Island. The ship track is shown in red and the ASIS buoy drift track in blue. R/V *Ronald Brown* departed Punta Arenas, Chile on 29 February 2008 (YD 59) and arrived in Montevideo, Uruguay on 12 April 2008 (YD 103). The ASIS buoy was deployed between 10 March to 18 March (YD 70 to 78).

(Compact Lightweight Aerosol Spectrometer) [see *Norris et al.*, 2008], installed on the mast with its intake 1 m below the sonic anemometer, provided measurements of aerosol concentrations and fluxes. These data will be discussed in future publications. The height of the sonic anemometer was 4.5 m above the mean water surface when the ASIS buoy was vertical. However, as shown in *Graber et al.* [2000, Figure 10b], the wind induced drag on the mast and deck results in a mean platform tilt which increases roughly as the square of the wind speed. This mean tilt, measured with a linear accelerometer (described below), reached a maximum of 23° during SOGaseX, and was modeled well by $Tilt = 0.028U_{10}^2 + 0.31U_{10} + 6.53$ where U_{10} is the mean 10 m wind speed, and $Tilt$ is in degrees from vertical. The tilt was accounted for in calculating the various instrument heights.

[11] A full motion package consisting of three orthogonally mounted rate gyros (Systron Donner GC1-00050-100), a tri-axis linear accelerometer (Columbia Research Laboratory SA-307HPTX) and a compass (Precision Navigation TCM-2) was installed in a water-tight housing roughly 7 m below sea level. The wind velocity was calculated by subtracting the measured platform motion from the anemometer signals following *Anctil et al.* [1994] and *Drennan et al.* [2003]. Following motion correction, the wind vector (u, v, w) was rotated so that u points into the mean wind direction, v is the cross-wind horizontal component and w is the vertical component, with $\bar{v} = \bar{w} = 0$ where the overbar denotes an average over the 30 min processing time used in the analysis.

[12] As the ASIS buoy's wind velocity was measured on a drifting platform, a possible correction for platform drift speed was considered. The ASIS drift velocity was calculated from the ARGOS positions using an averaging of order 3 h to remove noise in the positions. The mean platform drift varied between 1 and 4% (mean 2.3%) of the 10 m wind speed, consistent with the 3% surface drift current reported by *Wu*

[1975]. An exception occurred during 17 March (YD 77) when the wind speed dropped significantly for ten hours, and the ASIS buoy's drift speed reached 15% of U_{10} . The wind speed drop was accompanied by a nearly 90° shift in wind direction following the passage of a frontal system (visible in synoptic weather charts produced by the Australian Bureau of Meteorology, and available at www.bom.gov.au/australia/charts/archive/index.shtml; not shown here). During this short time period the ASIS buoy's drift was nearly perpendicular to the wind direction, with the buoy responding to the waves generated by earlier high winds. With the ASIS drift speed nearly equivalent to the estimated surface drift, no correction to the ASIS winds were made. Hence, the ASIS winds are measured with respect to the surface.

[13] Mean air temperature T_a and relative humidity RH were measured with a Rotronic MP101A-T7 sensor installed in a radiation shield at 3.5 m above mean water surface height. The relative humidity signal was reduced by 3% after comparison with the humidity measured on the *Ronald Brown* during the first three days of the experiment. Air temperature was also measured with a Brancker TR-1050 temperature logger. The two thermistors tracked each other very well until roughly 00Z on YD 76 (16 March). After this point the Rotronic humidity pegged at 97% (Figure 3e), its maximum given the 3% reduction, indicating probable wetting of the Rotronic probe. From YD 76 on the Brancker air temperature is used. Water temperature T_w was measured by a Brancker TDR-2050 temperature logger at a depth of 2 m. Water temperature and carbon dioxide were recorded by a SAMI-CO₂ sensor (Sunburst Sensors) mounted 1 m below the surface. See *Moore et al.* [2011] for details of the SAMI.

[14] Surface waves were measured with an array of eight capacitance wave gauges, each 3.5 m long by 1 mm diameter. Three gauges were installed around the perimeter of the ASIS buoy, with a fourth at the center. The data from these four

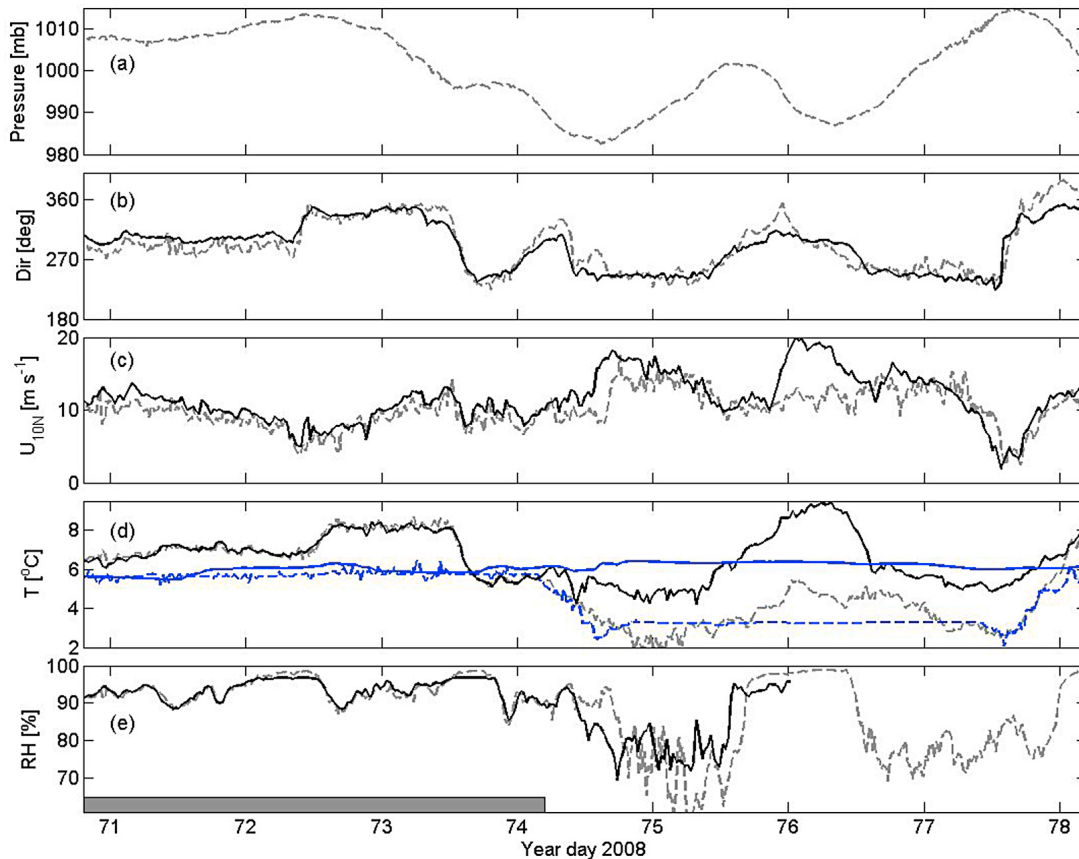


Figure 3. Summary of meteorological conditions during the ASIS buoy deployment. Solid (black) and dashed (gray) lines refer to measurements from the ASIS buoy and the R/V *Ronald Brown* respectively. The two were within 50 km of each other until 14 March (YD 74), as indicated by the shaded bar in the bottom panel. (a) Atmospheric pressure. (b) Wind direction. (c) 10 m neutral wind speed. (d) Air temperature and sea surface temperature (blue). (e) Relative humidity.

gauges, which formed a quadrilateral with sides of order 1 m, were corrected for platform motion to give true surface elevation, η . Significant wave height ($H_s = 4\langle\eta\rangle$, where $\langle\cdot\rangle$ denotes standard deviation) and peak frequency f_p were then calculated. Although the surface following capability of the ASIS buoy allows waves of order 5 m to be accurately registered, in some cases during SOGasex the buoy and its wave gauges were overtopped by large waves. In these cases a cubic spline correction was used to recreate the missing wave crests. This method was tested with good agreement by recreating wavecrests on a period without overshooting waves. During the period with the largest waves, up to 4% of the waves overtopped the staffs, with the largest corrections to individual waves being just over 1 m. However, the correction had little effect on the 30 min mean significant wave heights, 10 cm at most. Directional wave spectra were estimated using data from the four gauges via the Maximum Likelihood Method [see *Pettersson et al.*, 2003].

[15] All data, with the exception of the temperature loggers and SAMI, were recorded at 20 Hz on a custom-designed PC based logger located along with the motion package in an underwater housing at the base of the ASIS

buoy. Data were then analyzed in 30 min blocks. The eight day deployment yielded a total of 346 blocks of 30-min data.

3. Results

3.1. Meteorological Conditions During SOGasex

[16] The ASIS buoy deployment during SOGasex lasted only eight days but included two significant atmospheric depressions, as seen in Figure 3a. This plot shows atmospheric pressure as measured on the R/V *Ronald Brown*. Prior to 14 March (YD 74), and on 18 March (YD 78) the *Ronald Brown* was in close proximity of the ASIS buoy, typically within 50 km (see Figure 2). Between those times the *Ronald Brown* was to up to 300 km to the south of ASIS. As depressions on 14 and 16 March (YDs 74 and 76) passed to the south of both the *Ronald Brown* and the ASIS buoy, the pressure at ASIS was higher than indicated here. Based on synoptic charts provided by the Antarctic Meteorological Research Center at the University of Wisconsin-Madison (see, e.g., Figure 4) corrections were made ranging from under 4 hPa to 12 hPa.

[17] Wind speed and direction from both the ASIS buoy and the *Ronald Brown* are plotted in Figures 3b and 3c. Here

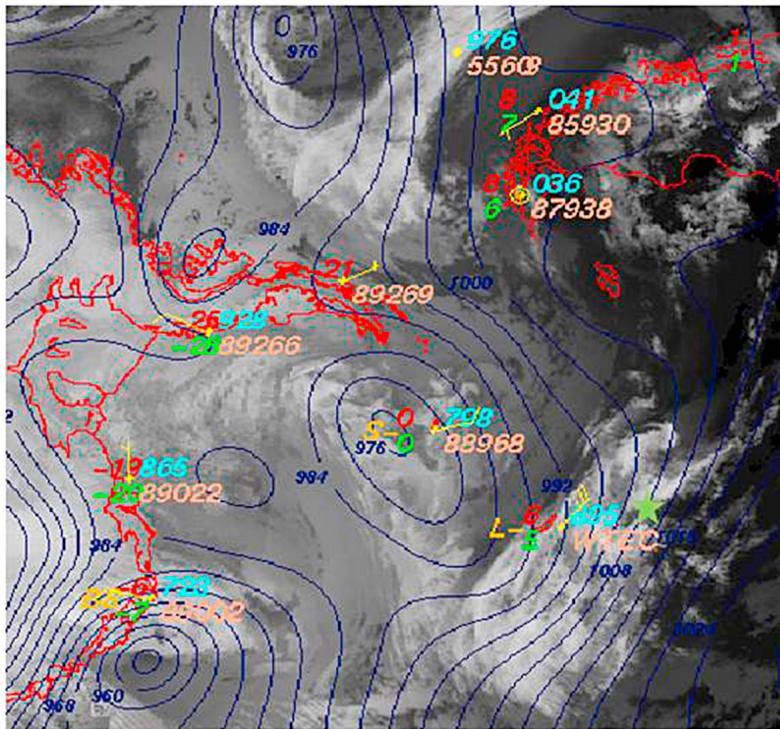


Figure 4. Synoptic chart of the experimental area from 06Z 16 March 2008 (YD 76). Note the 976 hPa storm centered to the SSW of the R/V *Ronald Brown* (station ID WTEC). The position of the ASIS buoy is indicated by the green star to the north (right) of the *Ronald Brown*. The analysis and composite imagery is provided by the Antarctic Meteorological Research Center, Space Science and Engineering Center at the University of Wisconsin-Madison.

the measured winds at roughly 4.5 m are brought to 10 m neutral equivalents U_{10N} using the stability functions of *Donelan* [1990], and logarithmic profile relations. The calculation of the Obukhov length L in the stability correction uses the *Smith* [1980] bulk expressions for the heat fluxes along with the measured friction velocity, u_* . u_* is calculated directly from the stress vector $\hat{\tau}$ as $u_*^2 = |\hat{\tau}|/\rho$ where

$$\hat{\tau} = \rho(-\overline{u'w'i} - \overline{v'w'j}). \quad (1)$$

Here ρ is air density, and the primes denote fluctuations of the variables about their means. During the three days of the deployment when the *Ronald Brown* was in the vicinity of ASIS, the ASIS buoy's 10 m winds were consistently 9% higher than those measured on the ship. The mismatch between the ASIS U_{10N} and R/V *Ronald Brown* U_{10N} will be discussed in section 4.

[18] The winds at the SOGasex were predominantly westerly, as expected, with maximum speeds of 18 and 20 m s^{-1} reached during the storms of 14 and 16 March (YD 74 and 76) respectively. For the first 36 h of the ASIS buoy deployment winds were from the WNW ($\sim 300^\circ$) and the atmosphere was moderately stable with T_a about 1° warmer than T_w (Figure 3d). A weak warm front passing over the domain on 12 March (YD 72.5) brought a shift of wind direction toward the south (from 340°) along with significantly warmer air. The period of stable stratification ended with the arrival of a cold front 24 h later. During this stable period the relative humidity was high, reaching 95% or higher (Figure 3e). The wind backed to

the WSW after the passage of the cold front bringing colder air to the ASIS buoy. This marks the beginning of the first unstable period of the experiment. A weak warm front passed early on 14 March (YD 74) quickly followed by a stronger cold front, which brought colder and drier air to the region. Following the passage of this front the wind speed increased to about 18 m s^{-1} . The first unstable period lasted until 15 March (YD 75) when again warmer air advected into the region.

[19] The frontal system passing on YD 75 was followed by a strong increase in wind speed. Following the cold front associated with the system, the wind again turned toward the WSW. During this storm the Rotronic measuring RH on ASIS failed and it did not function for the remainder of the experiment. The colder air advected in over the ASIS buoy after the cold front passed marks the beginning of the second unstable period lasting about 30 h until a new frontal system approached ASIS bringing warmer, stable air to the area.

3.2. Surface Fluxes

[20] As mentioned above, the momentum flux $\hat{\tau}$ was calculated from the measured wind velocity fluctuation time series. Time series and spectra for each run were first inspected, and occasional isolated spikes in the velocities or speed of sound channel were removed (interpolated through). Two characteristics were noted with the signals from the sonic anemometer. A noise floor was evident in most runs for frequencies above 3 Hz to 6 Hz. This was attributed to a grounding problem and was corrected by low-pass filtering

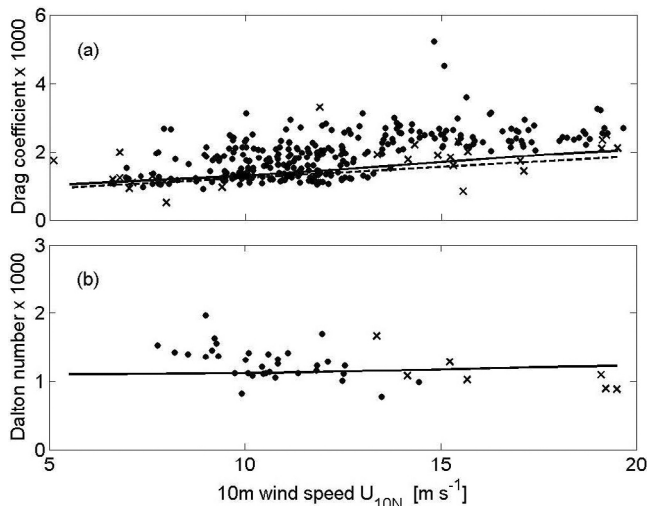


Figure 5. (a) Drag coefficient and (b) Dalton number, both 10 m neutral from the ASIS buoy during SOGasex (dots) and from aircraft during SOWEX (crosses) [Banner *et al.*, 1999]. The solid curves are the COARE 3.0 algorithm; the dashed line is Smith [1980].

the sonic data at 3 Hz. The effect on the measured friction velocities was 0.2% in the mean and under 1% for 2/3 of the valid cases. During the lull in the storm on 16 March (YD 76), during its decay on 17 March (YD 77), and during the low wind period on 12 March (YD 72), significant broad band noise was noted. These data, as well as a few highly nonstationary cases, were removed from the record, leaving 295 runs considered good.

[21] The 10 m neutral drag coefficient, defined as $C_{DN} = |\hat{\tau}|/\rho U_{10N}^2$ is plotted against 10 m neutral wind speed in Figure 5a. Also shown are the bulk relation curves of Smith [1980] and Fairall *et al.* [2003], as well as the SOWEX data of Banner *et al.* [1999]. SOGasex drag coefficients are significantly higher than predicted by the bulk relations in winds over $10 m s^{-1}$. We discuss this below in the context of the waves present at the site.

[22] The conditions during SOGasex played havoc with the Licor-7500 open path gas analyzer mounted on the ASIS buoy. As seen in Figure 6, during much of the ASIS deployment the humidity gradient $q_0 - q_{10}$ was near zero and was at times negative. Here q_0 is calculated from the sea surface temperature assuming saturation, with a 2% reduction due to salinity effects [Fairall *et al.*, 2003]. The low to negative humidity gradients are associated with stable atmospheric conditions, which accompanied winds with a northerly component (see Figure 3). During these periods the Licor-7500 was essentially non-operational with a near-zero or sporadic signal most of the time. This can likely be attributed to condensation on the sensor optics (note the fog in the background of Figure 1, taken shortly after deployment), which cannot easily be removed in an unattended system such as on the ASIS buoy.

[23] Only with the arrival of cool, drier air following the passage of a cold front on 13 March (YD 73) did the Licor data become usable. Even then, the humidity reported by the Licor remained lower than that reported by the Rotronic. This

was noticed during previous deployments of the Licor on ASIS buoys, and was attributed to salt accumulation on the Licor optics [Bogucki *et al.*, 2010]. We follow our earlier approach, and correct the gain of the Licor so that the mean humidity during a run matches that of the Rotronic. Unfortunately this limits the period of useful humidity flux data to the time the Rotronic was itself functional, i.e., before 16 March (YD 76). Even during the “good period” on 14 and 15 March (YDs 74 and 75) less than half the Licor data are usable, this time likely due to the abundance of spray accompanying the $17 m s^{-1}$ winds.

[24] Given these factors, and following a careful examination of all Licor time series and spectra, only 34 half hour runs of humidity were deemed usable. No carbon dioxide data from the Licor met the quality criteria. The bulk Dalton number was calculated as

$$C_{EN} = \overline{q'w'}/(U_{10N}(q_0 - q_{10N})) \quad (2)$$

where a Webb correction was applied to account for the fact that the Licor measures absolute humidity (the product of ρ and q) instead of specific humidity q [see Fairall *et al.*, 2003]. The Dalton numbers, plotted against wind speed in Figure 5b, are seen to agree well in the mean with the COARE3 bulk relation [Fairall *et al.*, 2003] and the SOWEX aircraft data of Banner *et al.* [1999]. The observed decrease in the SOGasex Dalton numbers with U_{10N} is small, but statistically significant (95% confidence). Clearly these data do not support a spray induced flux enhancement at high winds, although the quality controls on the Licor data may have eliminated data most affected by spray. That said, spray would have been a factor in all high wind runs. Finally the SOGasex data are consistent with the recent data of Drennan *et al.* [2007] collected during hurricanes.

3.3. Wave Conditions

[25] The wave conditions are summarized in Figure 7. H_s varied between 2 and 5.4 m. Maxima were reached in the two storms on 14–15 March (YD 74–75) and 16 March (YD 76), with individual waves reaching a maximum of 9.7 m peak to trough. In Figure 7b the directions for waves at the peak frequency, at 0.2 Hz and at 0.3 Hz are plotted, with wind direction included as a reference. The waves were predominantly moving toward E, traveling from directions between SW to NW. During the initial 36 h winds were fairly

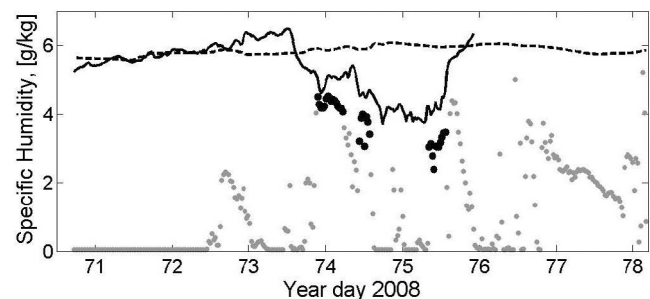


Figure 6. Specific humidity q_{10} from Rotronic (solid) and Licor (dots) hygrometers. The dashed line indicates saturated surface humidity q_0 based on the sea surface temperature. The black dots indicate Licor data considered usable.

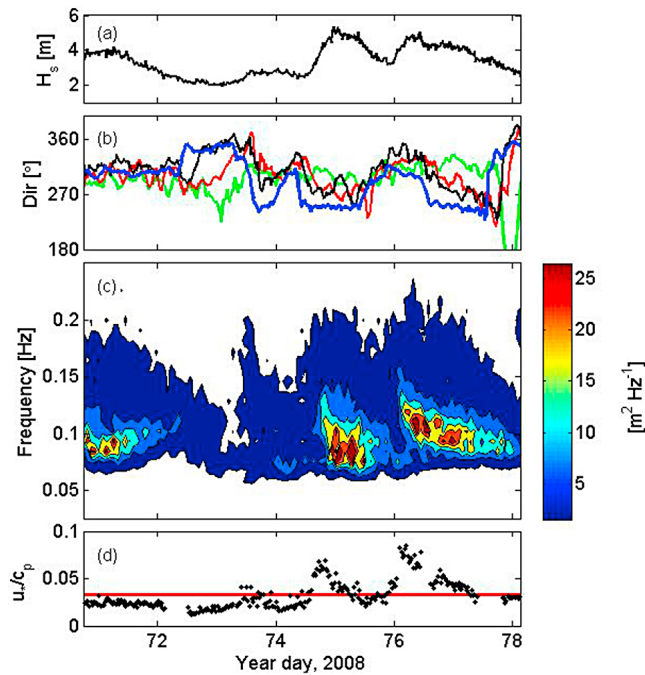


Figure 7. Wave measurements from the ASIS buoy. (a) Significant wave height, (b) Wind direction (blue) and wave directions for waves at the peak frequency (green), waves at 0.2 Hz (red) and waves at 0.3 Hz (black). (c) Time evolution of the 1-D wave spectra. (d) Inverse wave age, where the red line indicates the level for full development.

stationary, and all spectral components traveled close to the wind direction. A directional wave spectrum from this time is given in Figure 8a. During the following week, fronts accompanied by wind direction shifts of 60–90° passed through the region almost daily, and the wavefield was never again in equilibrium during the deployment. As expected, the shorter waves (0.3 Hz) respond more rapidly to a change in wind direction compared to the longer waves (0.2 Hz). However, except for the initial stationary period from 10 to 12 March (YD 70–72) and during the two storms, waves at the peak of the spectrum travel in directions that differ up to 60–100° from the wind direction.

[26] Figures 7c and 7d show the time evolution of the one-dimensional wave spectrum and the inverse wave age u^*/c_p , respectively, where c_p is the wave phase speed at the peak frequency. From Figure 7c it can be seen that the wave spectra displayed one single peak for most of the experiment. Note the increase in wind sea energy associated with increasing wind speed. Figure 7d reveals that, except during the two storm events, the wavefield was dominated by swell, i.e., $u^*/c_p < 0.033$. Even during the strong wind-forcing on 16 March (YD 76), u^*/c_p reached only 0.09.

[27] By including Figures 7c and 7d in the analysis of the wave direction at the peak frequency we can conclude that the peak waves are usually swell waves - not locally generated - which explains why their direction often deviates from the wind direction. These swells are generated by distant low pressure systems and arrive generally from WNW. Four examples of directional wave spectra normalized with the spectral level of the peak are presented in Figure 8. Except

for Figure 8b, these panels illustrate typical wave conditions for ASIS during the experiment, i.e., single peak spectrum and waves moving in roughly the same direction as the wind. Figure 8b illustrates one of very few cases when there was a clear spectral separation between the wind sea and swell.

3.4. Wave Analysis

[28] To put the SOGAsex wave measurements into a broader context they were analyzed together with wave measurements using ASIS buoys deployed during two other campaigns: the FETCH (Flux, État de la mer et Télédétection en Condition de fetch variable) experiment and the GasEx 2001 experiment. The FETCH experiment took place in the Mediterranean Sea, Gulf of Lion, from 12 March to 16 April 1998. An ASIS buoy was moored roughly 50 km offshore in a region known for its strong offshore Mistral winds. See Hauser *et al.* [2003] for an overview of the experiment and Drennan *et al.* [2003] for results from the ASIS buoy deployment. The measurements during GasEx 2001 were made from a drifting ASIS buoy in the equatorial Pacific during February–March 2001 [McGillis *et al.* 2004].

[29] Combining these three experiments yields an extensive data set containing 1556 individual measurements. These measurements were made in a wide range of wave regimes, from very young wind sea, in particular during

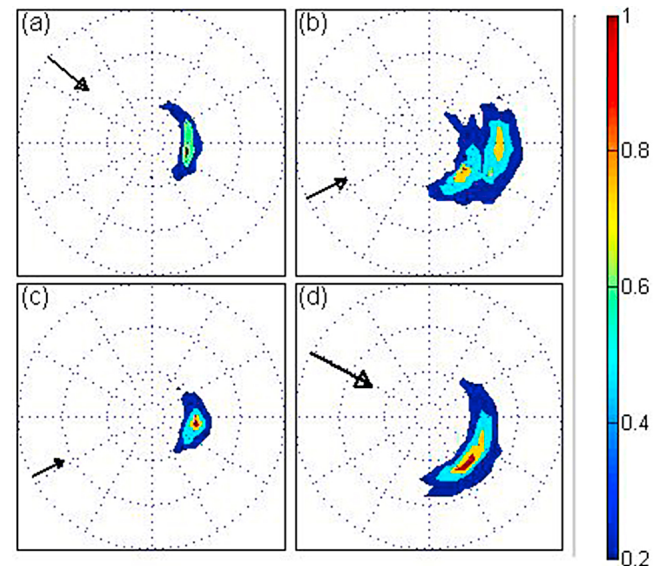


Figure 8. Four examples of individual 30-min average 2-D wave spectra. North and East are at top and right, respectively, of each panel. The dashed circles represent frequency bands from 0.1 to 0.4 Hz moving outward from the center. Spectral levels have been normalized by the peak value at each run, so that each plotted spectrum has a maximum of 1. The times, together with the peak spectral values (in parentheses), for each run are (a) YD 71, 02:16 UTC ($1.05 \text{ m}^2 \text{ Hz}^{-1}$), (b) YD 74, 15:41 ($0.35 \text{ m}^2 \text{ Hz}^{-1}$), (c) YD 75, 02:16 ($1.63 \text{ m}^2 \text{ Hz}^{-1}$) and (d) YD 76, 03:21 ($0.69 \text{ m}^2 \text{ Hz}^{-1}$). The arrows show wind direction. The length of the arrow indicates wind speed where the distance between successive dashed circles represents 10 m s^{-1} .

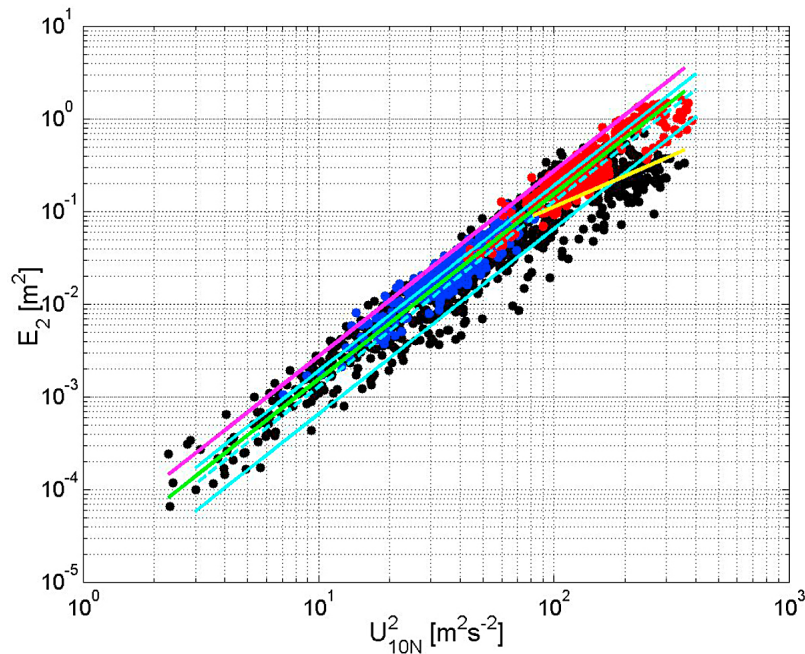


Figure 9. Wind wave energy E_2 as defined by equations (3) and (5) as a function of 10-m neutral wind speed squared. Dots represent individual measurements from SOGasex (red), FETCH (black) and GasEx 2001 (blue). The green line shows the mean value for all measurements. The magenta line shows E_2 calculated from PM64 spectra [Alves *et al.*, 2003]. The cyan lines show E_2 calculated using KC92 relations using $\tilde{X} = 8000$ where the upper line represents the unstable relation, the lower line represents the stable relation and the middle dashed line represents the combined relation. The yellow line is E_2 from the KC92 relation using the fetch limited relation with $\tilde{X} = 2180$.

FETCH, to swell dominated conditions. In this analysis we will be focusing on the energy associated with the wind sea part of the wave spectra. Spectral-energy based wave system partitioning methods [e.g., Gerling, 1992] often used to identify wind sea do not work well in following swell situations. Hence here the wind sea energy was calculated according to the method presented by Smedman *et al.* [2003], i.e., by separating each individual 1-D wave spectrum into two parts: one part associated with the wind sea, E_2 , and one part associated with longer waves, E_1 :

$$E_1 = \int_0^{n_1} S(n) dn \quad (3)$$

$$E_2 = \int_{n_1}^{\infty} S(n) dn \quad (4)$$

where $S(n)$ is the one-dimensional wave spectrum, n is frequency and n_1 is the separation frequency calculated as

$$n_1 = \frac{g}{2\pi \cdot 1.2 U_{10}} \quad (5)$$

where g is the acceleration of gravity. This definition of n_1 is somewhat different than the definition presented by Smedman *et al.* [2003]. In the original definition U_{10} was multiplied by a factor of $\cos \theta$, where θ is the difference between the wind and wave direction at the peak of the wave

spectrum. This term originates from the wave age parameter $c_p/(U_{10} \cos \theta)$, which according to the literature should take care of the part of the wind aligned in the direction of wave propagation. However, empirical studies have shown that the swell effects on the marine boundary layer e.g., wind profile, is similar for both swell traveling at 90° relative to the wind direction and wind-following swell [Smedman *et al.*, 2009; Höglström *et al.*, 2009]. Thus, inclusion of this term in the wave age definition may lead to erroneous classification of the sea state. The theoretical background for this is presented by Höglström *et al.* [2011].

[30] The inclusion of the factor 1.2 in the denominator of equation (5) also differs from the original definition of n_1 . The original definition separates the spectrum into two parts, waves moving faster and slower than the wind, i.e., n_1 is calculated from the relation $U_{10} = c_1 = g/(2\pi n_1)$, where c_1 is the wave phase speed at frequency n_1 . Here we instead separate the wave spectrum at the frequency representing full development, i.e., where $c_1 = 1.2 \cdot U_{10}$. With this separation E_1 represents the swell part of the spectrum and E_2 represents the waves influenced by the local wind.

[31] Figure 9 shows the expected variation of E_2 as a function of U_{10N}^2 . A similar plot of E_1 reveals that E_1 has no significant correlation with U_{10N}^2 , as expected (not shown). At the highest wind speeds the FETCH E_2 values level off and are smaller compared to the SOGasex data. This is consistent with the limited fetch conditions during FETCH, when the ASIS buoy was anchored only 50 km off the coast. This will be discussed further below.

[32] This set of data is well suited for re-visiting the formulations describing the asymptotic limits for fetch-limited wave growth. As a consequence of the similarity theory proposed by *Kitaigorodskii* [1962, 1973] the parameters total energy E_{tot} , H_s and f_p should be functions of the wind speed only. Applying dimensional analysis, the proportionality coefficients for total energy and peak frequency in the relations can be expressed as

$$\varepsilon = \frac{E_{tot} g^2}{U_{ref}^4} \quad (6)$$

$$\nu = \frac{f_p U_{ref}}{g} \quad (7)$$

where ε and ν are constants and U_{ref} is a reference wind speed. These equations describe the asymptotic limits for full development, i.e., the limits which the wind wave spectra approach during wave growth.

[33] *Alves et al.* [2003] revisit and reanalyze the classical experimental data presented by *Moskowitz* [1964] and *Pierson and Moskowitz* [1964], hereafter referred to as PM64. In PM64 the reference wind speed used in equations (6) and (7) is at 19.5 m. *Alves et al.* [2003] recalculate the PM64 expressions for the more typical reference wind speed of 10 m, which yields the following expressions for total energy of the analytical wind sea spectrum: $\varepsilon = 3.64 \times 10^{-3}$, and for peak frequency: $\nu = 0.13$.

[34] Using data from several field experiments including the Joint North Sea Wave Project (JONSWAP) experiment [*Hasselmann et al.*, 1973], from the Bothnian Sea [*Kahma*, 1981] and from Lake Ontario [*Donelan et al.*, 1985], *Kahma and Calkoen* [1992], hereafter referred to as KC92, studied the wave growth dependence on fetch and atmospheric stability. They propose expressions for ε and ν , each dependent on dimensionless fetch

$$\tilde{X} = gX/U_{10}^2 \quad (8)$$

where X is the fetch in m. There are separate expressions for stable and unstable atmospheric stratification, and a third combined expression.

[35] In order for a proper comparison between the observed E_2 values and parameterized values we have to take into account the fact that E_{tot} (equation (6)) is the total energy of a wind sea system, including all components of a wave system whose *peak* meets the requirement $2\pi n_p \geq g/(1.2 U_{10})$. E_2 , on the other hand, excludes components with $2\pi n < g/(1.2 U_{10})$ even if the associated wave peak satisfies $2\pi n_p \geq g/(1.2 U_{10})$. For the PM64 spectrum E_2/E_{tot} was calculated for wind speeds up to $U_{10} = 20 \text{ m s}^{-1}$ using equation (4). It was found that the ratio E_2/E_{tot} in this range was close to constant with $E_2/E_{tot} = 0.73 (\pm 2\%)$. In Figure 9 we include E_2 calculated from (6) using the PM64 value $\varepsilon = 3.64 \times 10^{-3}$ multiplied by 0.73. This PM curve is seen to represent well the outer envelope of the data, although it shows an overestimation by 77% above the mean of the observations, which is indicated by the green line in Figure 9. The mean of all observations presented here results in an ε of 1.5×10^{-3} (in terms of E_2 ; 2.1×10^{-3} in terms of E_{tot}).

[36] Also shown in Figure 9 is the E_2 calculated from the KC92 relations. When calculating E_2 from the KC92 equations we have used a dimensionless fetch of $\tilde{X} = 8000$, which was given by KC92 as the point where the relations should begin to approach fully developed conditions. Again, the factor of 0.73 is used to convert the calculated E_{tot} to E_2 in the fully developed limit. The KC92 prediction of E_2 in unstable fully developed conditions, being a factor of 2.9 greater than in stable fully developed conditions, is not supported by the data. Although the KC92 figures show a sharp transition between stable and unstable conditions, no such effect is observed in the data.

[37] Using $\tilde{X} = 8000$ the combined or unstable KC92 expressions are good approximations for both the SOGasex and GasEx 2001 data, as well as the low wind cases during FETCH. However, the high wind FETCH cases clearly deviate from the fully developed KC92 predictions. For most of these cases the wind was coming offshore. For typical FETCH mistral winds of $U_{10} = 15 \text{ m s}^{-1}$ with $X = 50 \text{ km}$, equation (8) yields $\tilde{X} = 2180$. Thus it is no surprise that the FETCH data during these conditions deviate from the SOGasex data in the same wind speed range. Recalculating E_2 from KC92 using the combined relation for the high wind FETCH cases results in the yellow line shown in Figure 9, which is a good fit to the observations. Note that the correction factor of 0.73 is not used to convert E_{tot} to E_2 in fetch limited conditions. Here the peak frequency is high enough that all wave components in the system have frequencies above the threshold (5), so that $E_{tot} = E_2$.

[38] The peak frequency is shown as a function of U_{10N} for the three experiments in Figure 10. Here only the wind sea dominated data from the experiments are included. The individual measurements have been colored according to their inverse wave age, u^*/c_p . Also shown in Figure 10 are the predictions from KC92, again using $\tilde{X} = 8000$ and calculated for both stable and unstable stratification and the combined expression. The green solid line shows the peak frequency calculated from (7) using $\nu = 0.19$, which is derived using the mean from all observations. This calculation shows a very good agreement with the KC92 prediction using the combined expression. The KC92 unstable relation tends to overestimate the peak frequency whereas the stable relation does a reasonably good job. The calculation of f_p using the *Alves et al.* [2003] recalculation of PM64, i.e., $\nu = 0.13$ (magenta line in Figure 10), yields an underestimation for U_{10N} less than 10 m s^{-1} but agrees well with the SOGasex data in the higher wind speed range.

[39] Most of the high wind FETCH data again deviate from the bulk of the measurements, which, as before, can be explained by the limited fetch. The thick black line shows the KC92 relation calculated using $\tilde{X} = 2180$, which fits the observations reasonably well. However, there is clearly a relation to the inverse wave-age; at a fixed U_{10N} , f_p is higher for younger seas compared to older (as expected).

4. Discussion and Conclusions

[40] An ASIS buoy deployed during SOGasex in 2008 measured wave conditions as well as near surface meteorological conditions and surface fluxes. The ASIS buoy drifted

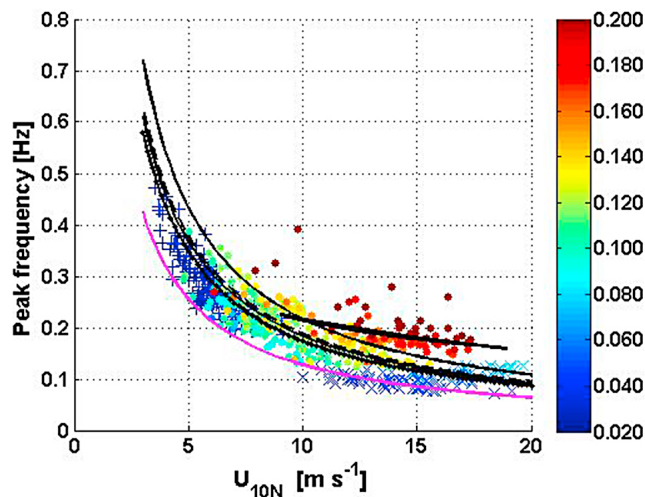


Figure 10. Peak frequency as a function of 10-m neutral wind speed U_{10N} . Symbols represent individual wind-sea measurements from SOGaseX (crosses), FETCH (circles) and GasEx 2001 (pluses). Symbol colors show the inverse wave age u^*/c_p of the measurements with values according to the color bar. The magenta line shows the calculated value of peak frequency using the PM64 spectra [Alves et al., 2003]. Black lines show f_p from the KC92 relation where the upper curved line represents the unstable relation, the lower line represents the stable relation and dashed middle line represents the combined relation. The green line represents the mean for all measurements. The straight black line shows f_p calculated using the fetch limited relations from KC92 with $\tilde{X} = 2180$.

in an easterly direction for eight days during which it encountered two storms with significant wave heights reaching 5.5 m and a maximum wind speed of 20 m s^{-1} . The atmospheric stratification during the deployment shifted between stable and unstable due to the frequent change of air mass, a feature typical at these latitudes.

[41] During the initial days after deployment mean meteorological measurements from the ASIS buoy were compared with those from the nearby *R/V Ronald Brown*. In general the comparison was good, however, the ASIS U_{10N} was consistently higher than the U_{10N} from *R/V Ronald Brown*. This was surprising as similar comparisons in other campaigns have consistently shown good agreement between ASIS winds and those from nearby vessels [e.g., Dupuis et al., 2003]. According to Edson et al. [2011] and references cited therein, the winds on the *Ronald Brown* are measured at 18 m above mean sea level, corrected for flow distortion following Fairall et al. [2003] and Dupuis et al. [2003], and brought to 10 m neutral equivalents using the COARE3 algorithm of Fairall et al. [2003]. Although the details of the COARE3 algorithm are somewhat different from those used here, these differences are too small to account for the observed discrepancies in wind speed. One possible factor was our use of measured u^* in the profile correction, whereas the COARE3 algorithm uses a bulk u^* . However, despite the differences between our measured and the COARE3 bulk friction velocities (recall Figure 5), the impact on U_{10N} was found to be at most 2%, and less than 1% for the comparison period.

[42] Our assumption that the velocity measured from the drifting ASIS buoy is the true wind velocity relative to the surface is another possible consideration. However, adding the drift speed to the measured wind speed would further increase the ASIS winds, and worsen the comparison with ship winds. Given that the drift speed of the drogued ASIS was found to be consistent with the expected wind-induced surface drift, our approach here seems reasonable. A third consideration is the offset in position between the ASIS buoy and ship during most of the comparison period. After deploying ASIS, the ship spent most of its time to the south of ASIS (see Figure 2b). The separation distance of order 20 km could account for at least part of the discrepancy.

[43] Finally, we note the possible influence of swell waves on the vertical wind speed profile. From field studies in the Baltic Sea it has been found that during swell dominated conditions (as during SOGaseX) the wind profile may be far from logarithmic [Smedman et al., 2009]. It exhibits a distinct ‘knee’ feature or even a very low level wind maximum in the height range 5–10 m. Below the maximum, or knee, the wind speed decreases rapidly toward the surface; above the knee the wind speed is more or less constant with height. This was found to be a result of the swell wave interaction with the atmospheric turbulence.

[44] Putting this into the context of SOGaseX, the ASIS measurements at 4.5 m were made in the region with a strong vertical gradient in the wind profile, and the *R/V Ronald Brown* wind measurements at 18.5 m were made at a level with a height constant wind profile. Thus, when calculating the 10 m neutral wind speed using traditional non-dimensional functions, the ASIS buoy measurements will overestimate the true 10 m wind speed and the *R/V Ronald Brown* measurements will underestimate the 10 m wind speed, i.e., the ASIS buoy U_{10N} would be higher than the *R/V Ronald Brown* U_{10N} , as observed. However, most studies of the swell-atmosphere interaction have been made in an unstable boundary layer. Little is known if it is similar during stable stratification which was the case during the three day comparison period.

[45] While the above discussion of waves focused on the wind sea component, the swell component was seen to have a significant effect on air-sea momentum transfer. In Figure 5 it is evident that the SOGaseX drag coefficients are significantly enhanced over previous bulk relations at high winds. Part of this relates to sea state. In Figure 11a, we plot u - w cospectra for eight consecutive 30-min runs at the peak of the storm early on 16 March (YD 76). During this time, wind was fairly steady at $U_{10N} = 16.7 \text{ m s}^{-1}$. The wavefield had a significant height of $H_s = 4.4 \text{ m}$ and a peak frequency of $f_p = 0.12 \text{ Hz}$. The inverse wave age of $U_{10N}/c_p = 1.29$ and directional spectrum (Figure 8d) indicate a wavefield near full development, with a small swell visible in the 1D wave spectrum (Figure 11b). In these conditions, the u - w cospectra, while showing considerable run to run variability, do not differ systematically from the universal cospectrum of Miyake et al. [1970]. This is consistent with Drennan et al. [1999] who showed that u - w cospectra over developing seas follow universal scaling.

[46] As the winds decay following the storm, the situation changes considerably. Figures 11c and 11d respectively show u - w cospectra and the mean 1D wave spectrum for a 4 h period at the end of day 76. The wind has dropped to

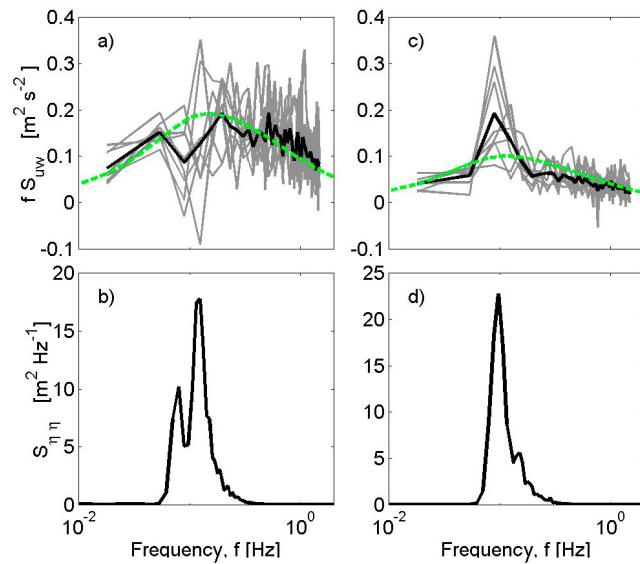


Figure 11. (a) Velocity u - w cospectra times frequency versus frequency for eight consecutive 30 min runs (gray lines) during 16 March (YD76.12–76.29). The black line shows the mean of the eight runs. The green dashed line shows the Miyake *et al.* [1970] universal spectrum rendered dimensional with mean values from the eight runs. Co-spectra have been multiplied by -1 for convenience. (b) Mean wave spectrum for period of Figure 11a. (c) Same as Figure 11a but for YD 76.85–77.02. (d) Mean wave spectrum for period of Figure 11c.

12.75 m s^{-1} and turned roughly 50 degrees (Figure 3b). H_s has dropped slightly to 4.2 m, with a peak frequency of 0.095 Hz, giving $U_{10N}/c_p = 0.78$ indicating swell. The cospectra no longer follow universal scaling, but include a significant additional peak at the swell frequency. This peak enhances the momentum flux by order 50% resulting in the consistently high drag coefficients observed during the decline of the storm. This enhancement is qualitatively consistent with Pacific swell cases observed during the Rough Evaporation Duct experiment at much lower wind speeds. In U. Höglström *et al.* (“Air-sea interaction features in the Baltic Sea and at a Pacific trade-wind site—An inter-comparison study,” submitted to *Boundary Layer Meteorology*, 2012) we further explore the mechanisms.

[47] The wind-wave energy, E_2 , from the ASIS buoy in SOGasex compared well with similar data from two other field experiments. When plotting the E_2 value as a function of U_{10N}^2 in a log-log representation the data display a positive slope of 2 indicating that the wave energy is proportional to U_{10N}^4 as predicted by similarity theory. The energy levels from these experiments in the open ocean and the Mediterranean are almost identical to the levels from measurements in the Baltic Sea presented by Smedman *et al.* [2003].

[48] Observations of wind sea wave energy from SOGasex and two other experiments were compared with the predictions from similarity theory. The similarity prediction of Alves *et al.* [2003] derived for fully developed seas was found to represent the upper bound of the measurements. The relations of KC92, applied at the suggested long-fetch limit, compare better with the data. This result is expected since the

Alves *et al.* [2003] prediction represents the asymptotic limit whereas the KC92 represent fully developed conditions. The measurements don’t support the KC92 result of stability dependent wind-wave energy; their combined relation compares very well with the mean of the field data presented here. The reduced slope of the FETCH data at the highest wind speeds was also successfully attributed to conditions with limiting fetch using the fetch dependent relations presented in KC92. The best fit to the observations results in a value of $\epsilon = E_{tot} g^2 U_{10N}^{-4} = 2.1 \times 10^{-3}$.

[49] The experimental data describing wind dependence of the peak frequency satisfies the similarity relations. The SOGasex data is well described by the similarity expression using ν from PM64 recalculated to a reference wind speed at 10 m by Alves *et al.* [2003], although using this ν for wind speeds lower than ca. 10 m s^{-1} slightly underestimates f_p . The best fit to the observations is achieved by $\nu = f_p U_{10N}/g = 0.19$. The combined and stable expressions from KC92 compare well with the mean experimental data over the full wind speed range whereas the unstable expression slightly overestimates f_p . Again, some of the scatter could be attributed to conditions with limiting fetch using the fetch dependent relations from KC92. Remaining scatter is most likely related to the wave-age where very young sea, far from full development, display a f_p at higher frequencies compared to older sea.

[50] **Acknowledgments.** We gratefully acknowledge NSF support for our participation in SOGasex (OCE-0726784). ES also acknowledges support from the Swedish Research Council Formas. We thank our fellow SOGasex PIs, as well as the efforts of the Captain and crew of the R/V Ronald Brown.

References

- Alves, J. H. G. M., M. L. Banner, and I. R. Young (2003), Revisiting the Pierson-Moskowitz asymptotic limits for fully developed wind waves, *J. Phys. Oceanogr.*, **33**, 1301–1323, doi:10.1175/1520-0485(2003)033<1301:RTPALF>2.0.CO;2.
- Anctil, F., M. A. Donelan, W. M. Drennan, and H. C. Graber (1994), Eddy correlation measurements of air-sea fluxes from a Discus buoy, *J. Atmos. Oceanic Technol.*, **11**, 1144–1150, doi:10.1175/1520-0426(1994)011<1144:ECMOAS>2.0.CO;2.
- Andreas, E. L. (1992), Sea spray and turbulent air-sea fluxes, *J. Geophys. Res.*, **97**, 11,429–11,441, doi:10.1029/92JC00876.
- Banner, M. L., W. Chen, E. J. Walsh, J. B. Jensen, S. Lee, and C. Fandry (1999), The Southern Ocean Waves Experiment. Part I: Overview and mean results, *J. Phys. Oceanogr.*, **29**, 2130–2145, doi:10.1175/1520-0485(1999)029<2130:TOWEP>2.0.CO;2.
- Bogucki, D., M.-E. Carr, W. M. Drennan, P. Woiceshyn, T. Hara, and M. Schmeltz (2010), Preliminary and novel estimates of CO_2 gas transfer using satellite scatterometer during the 2001GasEx Experiment, *Int. J. Remote Sens.*, **31**, 75–92, doi:10.1080/01431160902882546.
- DeGrandpre, M. D., R. Wanninkhof, W. R. McGillis, and P. G. Strutton (2004), A Lagrangian study of surface $p\text{CO}_2$ dynamics in the eastern equatorial Pacific Ocean, *J. Geophys. Res.*, **109**, C08S07, doi:10.1029/2003JC002089.
- Donelan, M. A. (1990), Air-sea interaction, in *The Sea*, vol. 9, *Ocean Engineering Science*, edited by B. LeMéhauté and D. Hanes, pp. 239–292, John Wiley, New York.
- Donelan, M. A., J. Hamilton, and W. H. Hui (1985), Directional spectra of wind-generated waves, *Philos. Trans. R. Soc. London, Ser. B*, **A315**, 509–562.
- Drennan, W. M., K. K. Kahma, and M. A. Donelan (1999), On momentum flux and velocity spectra over waves, *Boundary Layer Meteorol.*, **92**, 489–515, doi:10.1023/A:1002054820455.
- Drennan, W. M., H. C. Graber, D. Hauser, and C. Quentin (2003), On the wave age dependence of wind stress over pure wind seas, *J. Geophys. Res.*, **108**(C3), 8062, doi:10.1029/2000JC000715.
- Drennan, W. M., J. A. Zhang, J. R. French, C. McCormick, and P. G. Black (2007), Turbulent fluxes in the hurricane boundary layer. Part II: Latent heat flux, *J. Atmos. Sci.*, **64**, 1103–1115, doi:10.1175/JAS3889.1.

- Dupuis, H., C. Guerin, D. Hauser, A. Weill, P. Nacass, W. M. Drennan, S. Cloché, and H. C. Graber (2003), Impact of flow distortion corrections on turbulent fluxes estimated by the inertial dissipation method during the FETCH experiment on R/V *L'Atalante*, *J. Geophys. Res.*, *108*(C3), 8064, doi:10.1029/2001JC001075.
- Edson, J. B., C. W. Fairall, L. Bariteau, C. J. Zappa, A. Cifuentes-Lorenzen, W. R. McGillis, S. Pezoa, J. E. Hare, and D. Helmig (2011), Direct covariance measurement of CO₂ gas transfer velocity during the 2008 Southern Ocean Gas Exchange Experiment: Wind speed dependency, *J. Geophys. Res.*, *116*, C00F10, doi:10.1029/2011JC007022.
- Fairall, C. W., E. F. Bradley, J. E. Hare, A. A. Grachev, and J. B. Edson (2003), Bulk parameterization of air-sea fluxes: Updates and verification for the COARE algorithm, *J. Clim.*, *16*, 571–591, doi:10.1175/1520-0442(2003)016<0571:BPOASF>2.0.CO;2.
- Gerling, T. W. (1992), Partitioning sequences and arrays of directional ocean wave spectra into component wave systems, *J. Atmos. Oceanic Technol.*, *9*, 444–458, doi:10.1175/1520-0426(1992)009<0444:PSAAOD>2.0.CO;2.
- Graber, H. C., E. A. Terray, M. A. Donelan, W. M. Drennan, J. Van Leer, and D. B. Peters (2000), ASIS—A new-air-sea interaction spar buoy: Design and performance at sea, *J. Atmos. Oceanic Technol.*, *17*, 708–720, doi:10.1175/1520-0426(2000)017<0708:ANASI>2.0.CO;2.
- Gruber, N., et al. (2009), Oceanic sources, sinks, and transport of atmospheric CO₂, *Global Biogeochem. Cycles*, *23*, GB1005, doi:10.1029/2008GB003349.
- Harvey, M. J., et al. (2011), The SOLAS air-sea gas exchange experiment (SAGE) 2004, *Deep Sea Res., Part II*, *58*, 753–763, doi:10.1016/j.dsr2.2010.10.015.
- Hasselmann, K., et al. (1973), Measurements of wind-wave growth and swell decay during the Joint North Sea Wave Project (JONSWAP), *Dtsch. Hydrogr. Z.*, *12*, 1–95.
- Hauser, D., et al. (2003), The FETCH experiment: An overview, *J. Geophys. Res.*, *108*(C3), 8053, doi:10.1029/2001JC001202.
- Ho, D. T., C. S. Law, M. J. Smith, P. Schlosser, M. Harvey, and P. Hill (2006), Measurements of air-sea gas exchange at high wind speeds in the Southern Ocean: Implications for global parameterizations, *Geophys. Res. Lett.*, *33*, L16611, doi:10.1029/2006GL026817.
- Ho, D. T., C. L. Sabine, D. Hebert, D. S. Ullman, R. Wanninkhof, R. C. Hamme, P. G. Strutton, B. Hales, J. B. Edson, and B. R. Hargreaves (2011), Southern Ocean Gas Exchange Experiment: Setting the stage, *J. Geophys. Res.*, *116*, C00F08, doi:10.1029/2010JC006852.
- Högström, U., A. Smedman, E. Sahlée, W. M. Drennan, K. K. Kahma, H. Pettersson, and F. Zhang (2009), The atmospheric boundary layer during swell: A field study and interpretation of the turbulent kinetic energy budget for high wave ages, *J. Atmos. Sci.*, *66*, 2764–2779.
- Högström, U., A. Smedman, A. Semedo, and A. Rutgersson (2011), Comments on 'A global climatology of wind-wave interaction' by K. E. Hanley, S. E. Belcher and P. P. Sullivan, *J. Phys. Oceanogr.*, *41*, 1811–1813, doi:10.1175/JPO-D-10-05015.1.
- Iudicone, D., G. Madec, B. Blanke, and S. Speich (2008), The role of Southern Ocean surface forcings and mixing in the global conveyor, *J. Phys. Oceanogr.*, *38*, 1377–1400, doi:10.1175/2008JPO3519.1.
- Josey, S. A., E. C. Kent, and P. K. Taylor (1999), New insights into the ocean heat budget closure problem from analysis of the SOC air-sea flux climatology, *J. Clim.*, *12*, 2856–2880, doi:10.1175/1520-0442(1999)012<2856:NIITOH>2.0.CO;2.
- Kahma, K. K. (1981), A study of the growth of the wave spectrum with fetch, *J. Phys. Oceanogr.*, *11*, 1503–1515, doi:10.1175/1520-0485(1981)011<1503:ASOTGO>2.0.CO;2.
- Kahma, K. K., and C. J. Calkoen (1992), Reconciling discrepancies in the observed growth of wind-generated waves, *J. Phys. Oceanogr.*, *22*, 1389–1405, doi:10.1175/1520-0485(1992)022<1389:RDITOG>2.0.CO;2.
- Kitaigorodskii, S. A. (1962), Applications of the theory of similarity to the analysis of wind-generated wave motion as a stochastic process, *Izv. Akad. Nauk SSR, Geophys. Ser.*, *1*, 105–117.
- Kitaigorodskii, S. A. (1973), *The Physics of Air-Sea Interaction*, Isr. Program for Sci. Transl., Jerusalem.
- Liu, J., T. Xiao, and L. Chen (2011), Intercomparisons of air-sea heat fluxes over the Southern Ocean, *J. Clim.*, *24*, 1198–1211, doi:10.1175/2010JCLI3699.1.
- McGillis, W. R., J. B. Edson, J. D. Ware, J. W. H. Dacey, J. E. Hare, C. W. Fairall, and R. Wanninkhof (2001), Carbon dioxide flux techniques performed during GasEx-98, *Mar. Chem.*, *75*, 267–280, doi:10.1016/S0304-4203(01)00042-1.
- McGillis, W. R., et al. (2004), Air-sea CO₂ exchange in the equatorial Pacific, *J. Geophys. Res.*, *109*, C08S02, doi:10.1029/2003JC002256.
- Miyake, M., R. W. Stewart, and R. W. Burling (1970), Spectra and cospectra of turbulence over water, *Q. J. R. Meteorol. Soc.*, *96*, 138–143, doi:10.1002/qj.49709640714.
- Moore, T., C. Sabine, C. J. Zappa, W. McGillis, R. Hamme, R. Feely, and W. M. Drennan (2011), Sea surface pCO₂ and O₂ in the Southern Ocean during the austral fall, 2008, *J. Geophys. Res.*, *116*, C00F11, doi:10.1029/2010JC006560.
- Moskowitz, L. (1964), Estimates of the power spectrums for fully developed seas for wind speeds of 20 to 40 knots, *J. Geophys. Res.*, *69*, 5161–5179, doi:10.1029/JZ069i024p05161.
- Nightingale, P. D., G. Malin, C. S. Law, A. J. Watson, P. S. Liss, M. I. Liddicoat, J. Boutin, and R. C. Upstill-Goddard (2000), In situ evaluation of air-sea gas exchange parameterisations using novel conservative tracers, *Global Biogeochem. Cycles*, *27*, 2117–2120.
- Norris, S. J., I. M. Brooks, G. de Leeuw, M. H. Smith, M. Moerman, and J. J. N. Lingard (2008), Eddy covariance measurements of sea spray particles over the Atlantic Ocean, *Atmos. Chem. Phys.*, *8*, 555–563, doi:10.5194/acp-8-555-2008.
- Pettersson, H., H. C. Graber, D. Hauser, C. Quentin, K. K. Kahma, W. M. Drennan, and M. A. Donelan (2003), Directional wave measurements from three wave sensors during the FETCH experiment, *J. Geophys. Res.*, *108*(C3), 8061, doi:10.1029/2001JC001164.
- Pierson, W. J., and L. Moskowitz (1964), A proposed spectral form for fully developed wind seas based on the similarity theory of S. A. Kitaigorodskii, *J. Geophys. Res.*, *69*, 5181–5190, doi:10.1029/JZ069i024p05181.
- Smedman, A., X. G. Larsén, and U. Högström (2003), Effect of sea state on the momentum exchange over the sea during neutral conditions, *J. Geophys. Res.*, *108*(C11), 3367, doi:10.1029/2002JC001526.
- Smedman, A., U. Högström, E. Sahlée, W. M. Drennan, K. K. Kahma, H. Pettersson, and F. Zhang (2009), Observational study of the marine atmospheric boundary layer characteristics during swell, *J. Atmos. Sci.*, *66*, 2747–2763.
- Smith, S. D. (1980), Wind stress and heat flux over the ocean in gale force winds, *J. Phys. Oceanogr.*, *10*, 709–726, doi:10.1175/1520-0485(1980)010<0709:WSAHFO>2.0.CO;2.
- Speer, K., S. R. Rintoul, and B. Sloyan (2000), The diabatic Deacon cell, *J. Phys. Oceanogr.*, *30*, 3212–3222, doi:10.1175/1520-0485(2000)030<3212:TDDC>2.0.CO;2.
- Wanninkhof, R., K. F. Sullivan, and Z. Top (2004), Air-sea gas transfer in the Southern Ocean, *J. Geophys. Res.*, *109*, C08S19, doi:10.1029/2003JC001767.
- Woolf, D. K., and S. A. Thorpe (1991), Bubbles and the air-sea exchange of gases in near-saturated conditions, *J. Mar. Res.*, *49*, 435–466, doi:10.1357/002224091784995765.
- Wu, J. (1975), Wind-induced drift currents, *J. Fluid Mech.*, *68*, 49–70, doi:10.1017/S0022112075000687.